Available online at www.sciencedirect.com
SCIENCE DIRECT
Polymer 46 (2005) 5417–5427
polymer
www.elsevier.com/locate/polymer

Effects of processing history and annealing on polymorphic structure of nylon-6/montmorillonite nanocomposites

Shaobo Xie, Shimin Zhang*, Huiju Liu, Guangming Chen, Meng Feng, Huaili Qin, Fosong Wang, Mingshu Yang

Key Laboratory of Engineering Plastics, Joint Laboratory of Polymer Science and Materials, Institute of Chemistry, Chinese Academy of Sciences, Beijing 100080, People's Republic of China

Received 15 October 2004; received in revised form 28 February 2005; accepted 1 March 2005
Available online 4 May 2005

Abstract

The effects of processing history and annealing treatment on the thermal property and polymorphic structure of nylon-6/clay nanocomposites (NCNs) have been investigated. The nanocomposites, including intercalated and exfoliated ones, were prepared by extruding nylon-6 (N6) with sodium montmorillonite (Na-MMT) or organo-montmorillonite (OMMT), respectively. DSC analysis revealed multiple melting endotherms in either the extruded or the injection-molded N6 and NCNs samples. It has been observed that a small exothermic peak around 195 °C just before the lower melting peak in the skin regions. We demonstrated that this sub-T_m transition was directly related to the processing-induced shear stresses. WAXD analysis was further performed to characterize the polymorphic structure of injection-molded N6 and NCNs before and after annealing. Annealing at a temperature (80 °C) above the T_g of N6 resulted in increase of the absolute content of γ-form in the skin regions and of the relative content of γ-form in the core regions of NCNs. In particular, annealing only leaded to increase the fraction of γ-form in the exfoliated N6/OMMT nanocomposites, which might be related to a confining effect of MMT platelet on the polymer chains mobility.

Keywords: Nylon-6; Nanocomposite; Crystal structure

1. Introduction

In recent years, polymer/clay nanocomposites consisting of layered silicates, such as montmorillonite (MMT), have attracted much attention from both industry and academia. The interest stems from the fact that nano-sized-layer-filled polymers can exhibit dramatic improvement in mechanical and thermal properties with as little as 5 wt% clay content because of the strong synergistic effects between the polymer and the silicate platelets on molecular or nanometric scale [1]. Nylon-6/clay nanocomposites (NCNs), pioneered by Toyota researchers, have extensively been investigated during the last decade (see Ref. [1,2] and references therein). The NCNs containing a small amount of clay exhibits superior properties such as high modulus, high strength, high heat distortion temperature (HDT), good gas barrier properties and flame retardancy. The origin of the enhanced properties of NCNs is presumably thought to be not only from the dispersion of 1-nm-thick clay layers within the nylon-6 matrix, but also from the strong interaction between the macromolecules and the nanometric filler layers which possess high surface area and aspect ratio [2].

Nylon-6 (N6) is a high-performance semi-crystalline polymer. The crystal structure and polymorphism of N6 have been extensively studied [3,4]. N6 has a complicated polymorphic structure that exhibits two major crystal forms, namely monoclinic α-form and monoclinic or pseudohexagonal γ-form depending on the thermal history, processing conditions, mechanical stress, crystallization conditions and so on. The principal difference between the two forms is the molecular packing. In the more thermodynamically stable α-form, hydrogen bonds are formed between anti-parallel chains. In the γ-form, molecular chains have to twist away

* Corresponding author. Tel.: +86 10 82615665; fax: +86 10 62559373.
E-mail address: smzhang@iccas.ac.cn (S.M. Zhang).

0032-3861/$ - see front matter © 2005 Elsevier Ltd. All rights reserved.
doi:10.1016/j.polymer.2005.03.094

from the zigzag planes to form hydrogen bonding between parallel chains. The α-form is commonly resulted from slowly cooling from the melt state, while the γ-form is typically obtained in uniaxial deformation such as high-speed spinning or by cooling the samples rapidly from the melt state [5]. Since the discovery of NCNs, the influence of the clay platelets on the crystal structure of N6 has also been studied. It is well recognized that the layered silicates can promote growth of the γ-form crystalline of N6 [6–12]. In the NCNs, the γ-form is preferentially in the proximity of the silicate layers, whereas the α-form exists away from the polymer–clay interphase region [13,14]. The clay layers were shown to orient along the direction of shear, causing orientation of the polymer chains as well [10].

In general, processing history and annealing treatment will determine the relative fraction of the crystalline polymer phases in semi-crystalline polymer nanocomposites, and thus may have significant influence on the mechanical and other properties of nanocomposites. However, the effects of processing history on the polymorphic structure of injection-molded NCNs have not been fully understood; in fact, limited studies have been reported [11, 14–16]. Not only early studies by Toyota researchers [7] but also recent NMR studies [11,14] showed significant variations in γ/α ratio throughout an injection-molded specimen, reflecting variation in processing history. It was also found that thermal history, such as annealing (at 214 °C) after injection molding, had a dramatic influence on γ/α crystal structure ratio [14]. We are aware that prior to mechanical testing, annealing of injection-molded NCNs specimens at 70–90 °C [17,18] or not [19,20] has been reported. But the question is whether and how the annealing treatment has influence on the thermal and mechanical properties of NCNs. As far as we know, there is no in-depth study in the literature on the effect of annealing within such a range of temperature on the crystallization behavior and crystal structure of injection-molded NCNs.

In this paper, we prepared N6/Na-MMT and N6/OMMT nanocomposites. The influences of processing history and annealing on the polymorphic structure of pure N6 and the corresponding NCNs are discussed toward providing insight into the structure–properties relationship of NCNs. Differential scanning calorimetry (DSC) and wide angle X-ray diffraction (WAXD) were used to provide detailed information on the crystal structure of pure N6 and NCNs before and after annealing at 80 °C.

2. Experimental

2.1. Materials

Nylon-6 (N6) homopolymer resin (Capron® 8200 NL) with a density of 1.13 g/cm^3 was generously donated by Honeywell Nylon System (China). Sodium montmorillonite (Na-MMT), with a cation-exchange capacity of 85 meq/100 g, was purchased from Zhangjiakou Qinghe Chemical Plant Co. (China). Octadecyl diethanolamine was supplied by Shanghai Jinshan Chemical Co. (China). Other reagents were of commercial products and used as received.

The organo-montmorillonite (OMMT) was prepared by cation-exchange reaction with octadecyl diethanolamine salt formed by protonizing the amine. Octadecyl diethanolamine (15 g, 42.5 mmol) and equivalent hydrochloric acid (37 wt% solution in water) were mixed to prepare the amine salt. Na-MMT (50 g) was dispersed vigorously and swelled in 1 L of deionized water at 80 °C. The amine salts were dropwise added to the slurry. After stirring vigorously at 80 °C for 3 h, the precipitate was collected at ambient temperature, washed thoroughly with a warm water/ethanol (1:1 by volume) mixture until no Cl^- could be detected by 0.1 mol/L of $AgNO_3$ solution. The yielded OMMT was dried under vacuum at 80 °C for 8 h and then ground to fine powders with diameters of 40–70 μm.

2.2. Preparation of NCNs

The NCNs were prepared with a twin-screw extruder (Nanjing Rubber and Plastics Machinery Plant, SHJ-30, China) with a 30-mm diameter and an *L/D* ratio of 23. The screw speed was 200 rpm and the temperature of the extruder was maintained at 210, 220, 230, and 230 °C from hopper to die, respectively. The extrudates were pelletized at the die exit, dried, and injection-molded into 4-mm-thick standard Izod bars (ASTM D256) with an injection-molding machine (SZ-68/400, Chende Plastic Machinery, China) at mold temperature of 60 °C. In the following discussion, pure pristine N6 (i.e. without MMT) sample is called PA1. NCNs generated from N6 and Na-MMT or OMMT are denoted PA2 or PA3, respectively. The exact amount of MMT in PA2 or PA3 was determined by placing pre-dried extruded pellets in a furnace at 900 °C for 45 min and weighing the residual ash [20]. The results were corrected for loss of structural water. The weight percentage of MMT in the NCNs was calculated from the following formula [20]:

$$\%\mathrm{MMT} = \frac{\%\mathrm{MMT_{ash}}}{0.935} \quad (1)$$

where $\%\mathrm{MMT_{ash}}$ is the mass fraction after incineration relative to the original nanocomposite mass. The weight fraction of MMT in NCNs is 2.4 and 2.9 wt% for PA2 and PA3, respectively. Prior to extruding and injection molding, the pellets were dried under vacuum at 85 °C for at least 12 h to avoid moisture induced degradation reactions. After injection molding, the Izod bars were immediately sealed and placed in a desiccator prior to annealing treatment.

2.3. Annealing treatment and skin–core sample preparation

The as-molded 4-mm-thick Izod bars of PA1, PA2 and PA3 were undergone for annealing treatment. The treatment was performed under vacuum at 80 °C (above the T_g of N6,

that is about 50 °C) for 6 h and then slowly cooled to room temperature under vacuum. The reference sample bars, designated also as non-annealed ones hereafter, were placed under vacuum at room temperature for 12 h. Similar to the method described by Fornes et al. [15], the skin or core region of injection-molded specimens, as shown in Fig. 1, was obtained by removing 0.2 or 2 mm from annealed/non-annealed Izod bars, respectively. The detailed sample information is shown in Table 1.

2.4. Preparation of samples for DSC

The extruded pellets and injection-molded Izod bars were used for DSC analysis. The extruded PA1, PA2 and PA3 pellets and three kinds of pure N6 samples with different processing history were dried under vacuum at 85 °C for at least 12 h prior to DSC measurements. Three kinds of pure N6 samples with different processing history are as-received N6, quenched N6, and extruded N6 in CS-183. The quenched N6 was prepared by melting the as-received N6 at 230 °C for 2 min under quiescent conditions and then quenched to room temperature. The extruded N6 in CS-183 was prepared by melting the as-received N6 in CS-183 MMX Mini Molder (Custom Scientific Instruments, Inc.) at 230 °C for 2 min under shear conditions, then extruded and quenched to room temperature. These two different processing histories could mimic the extrusion in twin-screw extruder, but with different shear stress. There are gradually increased shear stresses from the quenched N6 (without shear stress) to the extruded N6 in CS-183, then to the extruded N6 in twin-screw extruder (i.e. PA1).

In addition, slices about 30 μm thick were cut with a microtome (Leica RM2515, Leica Microsystem Ltd.) from the skin or core regions of annealed/non-annealed injection-molded bars, and directly analyzed.

2.5. Characterization

Wide-angle X-ray diffraction (WAXD) patterns were obtained using a Rigaku D/max 2400 diffractometer (40 kV, 200 mA; Cu Kα, $\lambda = 0.154$ nm; reflection mode). WAXD scans were performed on the injection-molded Izod bars, as well as on Na-MMT and OMMT powder, at ambient temperature with a 2θ range between 1.5 and 40°, at a scanning rate of 4°/min and a scanning step of 0.02°. The skin region (i.e. top 0.2 mm removed) and the core region (i.e. top 2 mm removed) of the Izod specimens were oriented such that the incident beam reflects off the major face, as depicted in Fig. 1.

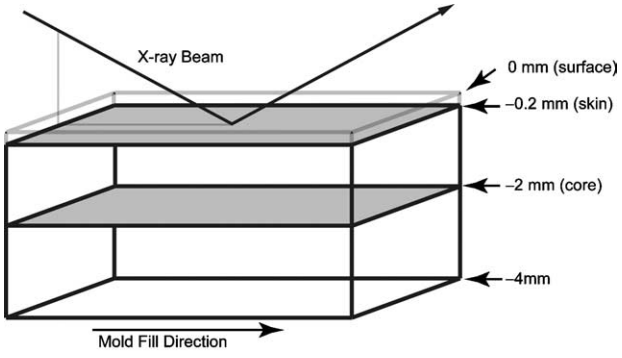

Fig. 1. Illustration of WAXD geometry and skin–core locations.

The morphology of the NCNs was investigated by a Hitachi H-800 transmission electron microscope (TEM) apparatus at an acceleration voltage of 200 kV. Ultra-thin sections were obtained by cryogenic ultramicrotoming the injection-molded samples along the injection direction.

Differential scanning calorimetry (DSC) analyses were carried out on a Perkin–Elmer DSC-7 differential scanning calorimeter thermal analyzer in a nitrogen environment. The sliced samples (approximately 7 mg) were heated at a rate of 20 °C/min from −10 to 280 °C and held at 280 °C for 10 min to eliminate the influence of thermal history, then cooled at a rate of 20 °C/min to −10 °C. On the second heating run, the samples were heated from −10 to 280 °C at a rate of 20 °C/min.

3. Results

3.1. Nanostructure of NCNs

Fig. 2 shows the WAXD patterns of MMT (Na-MMT and OMMT) and their corresponding NCNs (PA2 and PA3). The directly compounded PA2 reveals an increased

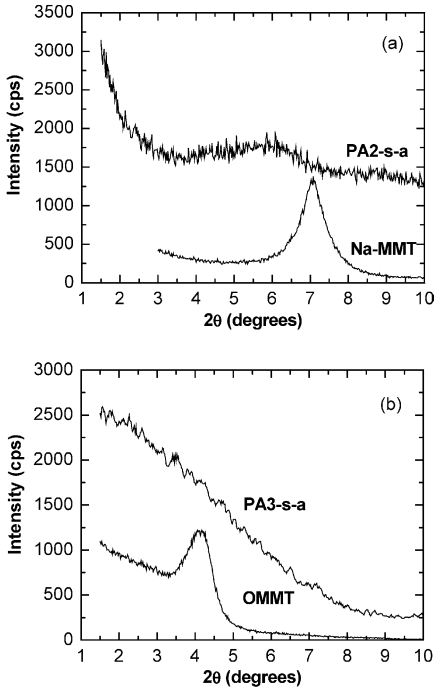

Fig. 2. WAXD patterns. (a) Na-MMT and corresponding nanocomposites PA2, (b) OMMT and corresponding nanocomposites PA3. The curves are vertically offset for clarity.

Table 1
Sample information used for DSC and WAXD investigation

Sample	Filler	MMT content (wt%)[a]	Code[b]	Location	Annealing
PA1	–	0	PA1-s-na	Skin	No
			PA1-s-a	Skin	Yes
			PA1-c-na	Core	No
			PA1-c-a	Core	Yes
PA2	Na-MMT	2.4	PA2-s-na	Skin	No
			PA2-s-a	Skin	Yes
			PA2-c-na	Core	No
			PA2-c-a	Core	Yes
PA3	OMMT	2.9	PA3-s-na	Skin	No
			PA3-s-a	Skin	Yes
			PA3-c-na	Core	No
			PA3-c-a	Core	Yes

[a] From Formula (1) as described in Section 2.2.
[b] The designations applied to the NCNs codes are as follows: 'PA*n*-x-y' where *n* refers to the sample code (*n* = 1 stands for 'PA1', and so on), x refers to the skin/core regions (x = s stands for skin region of injection-molded sample and x = c stands for core region), and y refers to annealing treatment (y = a stands for annealed and y = na for non-annealed).

d-spacing (from 1.24 nm of Na-MMT to 1.5 nm of PA2, Fig. 2(a)), indicating that N6 polymer has entered the clay gallery. When using OMMT (d_{001} = 2.1 nm), the resultant PA3 exhibits pattern of decreasing intensity with increasing 2θ (Fig. 2(b)), suggesting good dispersion of MMT. Actually, MMT platelets have been exfoliated within N6 matrix in monolayers [21].

The TEM images shown in Fig. 3 provide direct evidence of the conclusions from the WAXD data. The intercalated nanostructure of N6/Na-MMT (PA2) is present in Fig. 3(a), where the intercalated MMT stacks are orientated along the mold fill direction. For the N6/OMMT (PA3) sample, a well-exfoliated nanostructure consisting largely of individual clay platelets distributed throughout the N6 matrix can be obviously seen from Fig. 3(b). The distances between exfoliated clay platelets are 20–40 nm. Individual MMT sheets also orient along the injection molding direction.

The WAXD patterns of PA2 and PA3 shown in Fig. 2 correspond to the skin regions of the injection-molded bars (PA2-s-a and PA3-s-a). When WAXD experiments were carried out on the core regions, the patterns changed. As shown in Fig. 4, both PA2-c-a and PA3-c-a do not show any peaks at $2\theta = 1.5$–10°, differing from the corresponding skin curves. It seems that there is an orientated distribution of MMT platelets in the injection-molded NCNs specimens from skin to core region. Kojima et al. [7] reported a preferred orientation of MMT platelets in injection-molded NCNs. The anisotropic MMT platelets were primarily oriented in the flow axis during injection molding. The MMT monolayers were parallel to the bar surface in the skin region, while in the core region they were randomly oriented

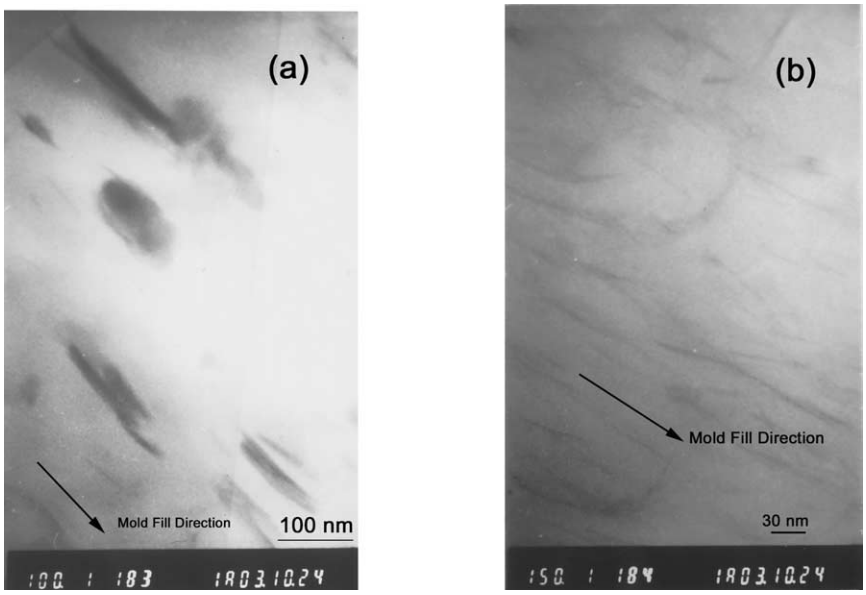

Fig. 3. TEM images of NCNs taken close to the surface region: (a) PA2 and (b) PA3.

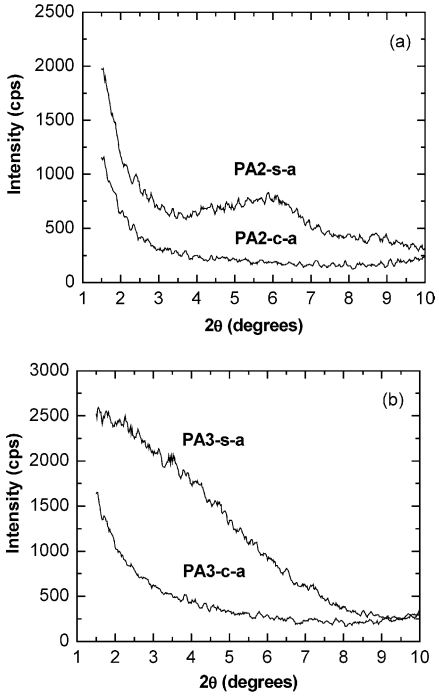

Fig. 4. WAXD patterns of skin and core region of (a) PA2 and (b) PA3.

around the flow axis, but not parallel to the bar surface. Reflected in WAXD curves, the intensity of diffraction peak in low angles decreased greatly form skin to core region. Therefore, the preferred orientation of single clay platelets in exfoliated PA3 can be expected from Figs. 3(b) and 4(b). Similar orientated distribution of MMT platelets has been reported [22,23]. The characterless WAXD pattern in PA2-c-a maybe merely represents the randomly oriented intercalated structure in the core region of PA2, rather than an exfoliated structure [24].

3.2. DSC results

Fig. 5(a) and (b) presents the DSC curves of samples taken from the core and skin regions of non-annealed injection-molded PA1, PA2 and PA3 bars, respectively. The melting peaks around 220 °C are present for all samples, no matter whether in core or skin regions. In the core region (Fig. 5(a)), a small low temperature endothermic peak around 210 °C is observed only for samples containing clay (PA2 and PA3). In the skin regions (Fig. 5(b)), the peak at 210 °C is more obvious, even in the pure N6 sample (PA1). The incorporation of clay increases the area under the peak at 210 °C and reduces the area under the peak at 220 °C. Another obvious difference in the melting endothermic curves between the core and skin regions lies in that a small exothermic peak around 195 °C (just before the low-temperature melting peak) is observed in the skin region, which is absent in the core region. This sub-T_m transition in nylons was also noticed previously by Khanna et al. [25].

The melting endothermic curves of annealed samples are shown in Fig. 5(c) and (d). It is evident that the thermodynamic profiles did not vary after the annealing treatment at 80 °C for 6 h in both of the core regions (Fig. 5(c)) and the skin regions (Fig. 5(d)) in comparison with the corresponding non-annealed samples.

The DSC cooling scans of non-annealed injection-molded PA1, PA2 and PA3 are shown in Fig. 6. It can be seen that regardless of the locations selected, the exothermic peak of N6 crystallization of PA3 appears almost at the same temperature as that of pure N6 (PA1) while that of PA2 reveals a shift of about 3 °C towards higher temperature. The DSC cooling scans of annealed samples present results similar to the non-annealed samples.

Considered the complexity of measuring the crystallinity by DSC in the presence of the sub-T_m exothermic transition [26], the crystallinity ($X_{C\text{-}DSC}$) of injection-molded samples was calculated from the enthalpy evolved during crystallization based on the cooling scans, using the following formula [27]:

$$X_{C-DSC}(\%) = \frac{\Delta H_C}{(1-\phi)\Delta H_m^0} \times 100 \quad (2)$$

where ΔH_C is the apparent enthalpy of crystallization of sample, ΔH_m^0 is the extrapolated value of the enthalpy corresponding to the melting of 100% crystalline pure N6, which is taken as 190 J/g [27,28], and ϕ is the weight fraction of MMT in the NCNs. The melting peak temperature (T_m), the peak temperature of crystallization (T_c), ΔH_C, and corresponding $X_{C\text{-}DSC}$ of the various samples are presented in Table 2. The crystallinity value was estimated similar in all cases from the calorimetric data, regardless of pure N6 (PA1) or NCNs (PA2, PA3) and skin region or core region, with a smaller value found in PA3 sample. Annealing usually leads to an improvement of crystallinity and crystal perfection. It can be seen from Table 2 that annealing at 80 °C increased the degree of crystallinity more or less, while the T_m and T_c seem to be affected to a lesser extent by the annealing treatment.

Table 2
DSC data for injection-molded N6 samples

Sample	T_m (°C)	T_c (°C)	ΔH_C (J/g)	$X_{C\text{-}DSC}$ (%)
PA1-s-na	211.3/220.1	183.3	−64.2	33.8
PA1-s-a	213.3/221.8	183.8	−67.4	35.5
PA1-c-na	221.1	183.1	−65.9	34.7
PA1-c-a	221.1	183.2	−66.5	35.0
PA2-s-na	211.2/220.1	186.2	−62.2	33.6
PA2-s-a	212.1/221.1	185.8	−64.0	34.5
PA2-c-na	209.4/220.5	186.0	−64.2	34.6
PA2-c-a	220.8	185.8	−65.2	35.2
PA3-s-na	211.6/221.1	182.6	−57.4	31.1
PA3-s-a	211.3/220.8	182.8	−58.6	31.8
PA3-c-na	220.7	183.2	−57.9	31.4
PA3-c-a	219.4	182.0	−58.1	31.5

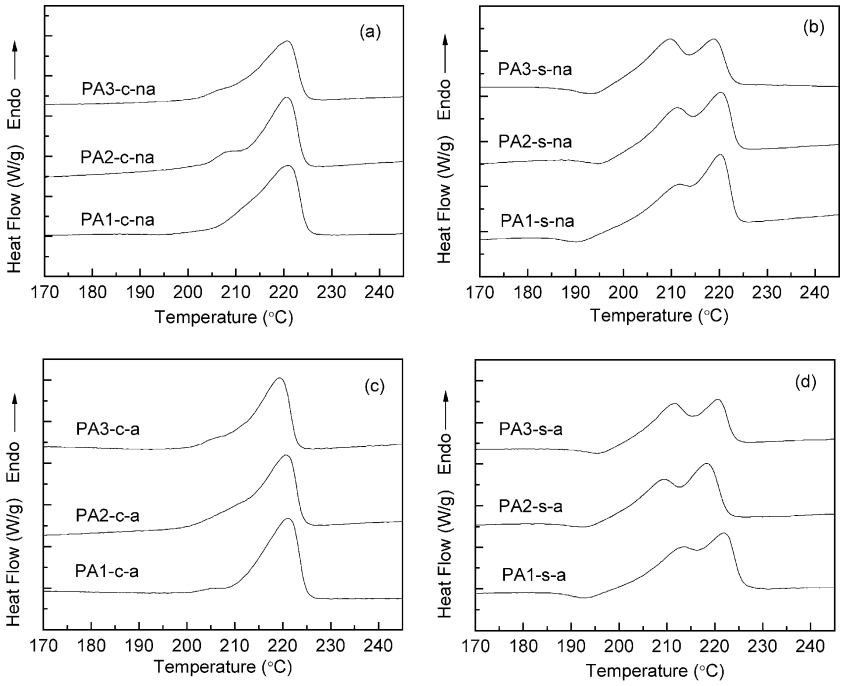

Fig. 5. DSC heating scans of samples taken from the core (a, c) and skin (b, d) of non-annealed/annealed injection-molded PA1, PA2 and PA3 bars. The curves are vertically offset for clarity.

3.3. WAXD analyses

In order to check the influences of processing and subsequently annealing on the crystal structure of injection-molded N6 sample, WAXD measurements were performed on the skin and core regions of both annealed and non-annealed samples, as shown in Fig. 7. The peaks at $2\theta \approx 20.2°$ ($\alpha 1$) and 23.4° ($\alpha 2$) are assigned to (200) and (202)+(002) planes of α-form, respectively; while the peaks at $2\theta \approx 11.0$ and 21.3° are assigned to (020) and (200)+(001) planes of γ-form, respectively [23]. From Fig. 7, it can be clearly observed that the α-form is predominant in the core region of injection-molded part, while the γ-form is the only crystalline form of N6 in the skin region. Similar observations have been reported on injection-molded N6 samples [15,16,23]. This probably reflects the higher cooling rates in the skin region, where crystallization at lower temperature hindered or retarded polymer chain mobility favoring γ-form [29], than the core region.

The WAXD patterns of N6 samples can be deconvolved into five components by approximating peaks with Gaussian curves following the work by Gurato et al. [30]. The five components consist of $(020)_\gamma$, $(200)_\gamma$, $(200)_\alpha$, and $(002)_\alpha$ diffraction peaks appearing at $2\theta = 11.0$, 21.3, 20.2, and 23.4°, respectively, and a broad peak due to the amorphous component. Therefore, the total relative crystallinity ($X_{\text{C-WAXD}}$) and the fractions of α- and γ-from ($X_{\alpha\text{-WAXD}}$ and $X_{\gamma\text{-WAXD}}$) can be calculated from Formula (3)–(5),

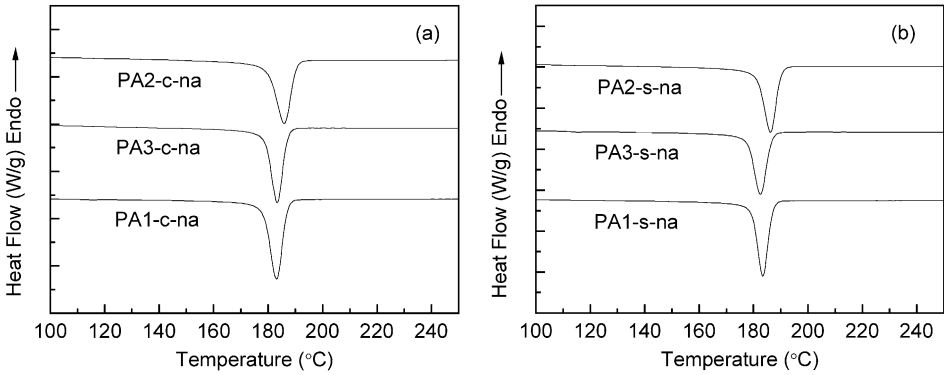

Fig. 6. DSC cooling scans of samples taken from the core (a) and skin (b) of non-annealed injection-molded PA1, PA2 and PA3 bars. The curves are vertically offset for clarity.

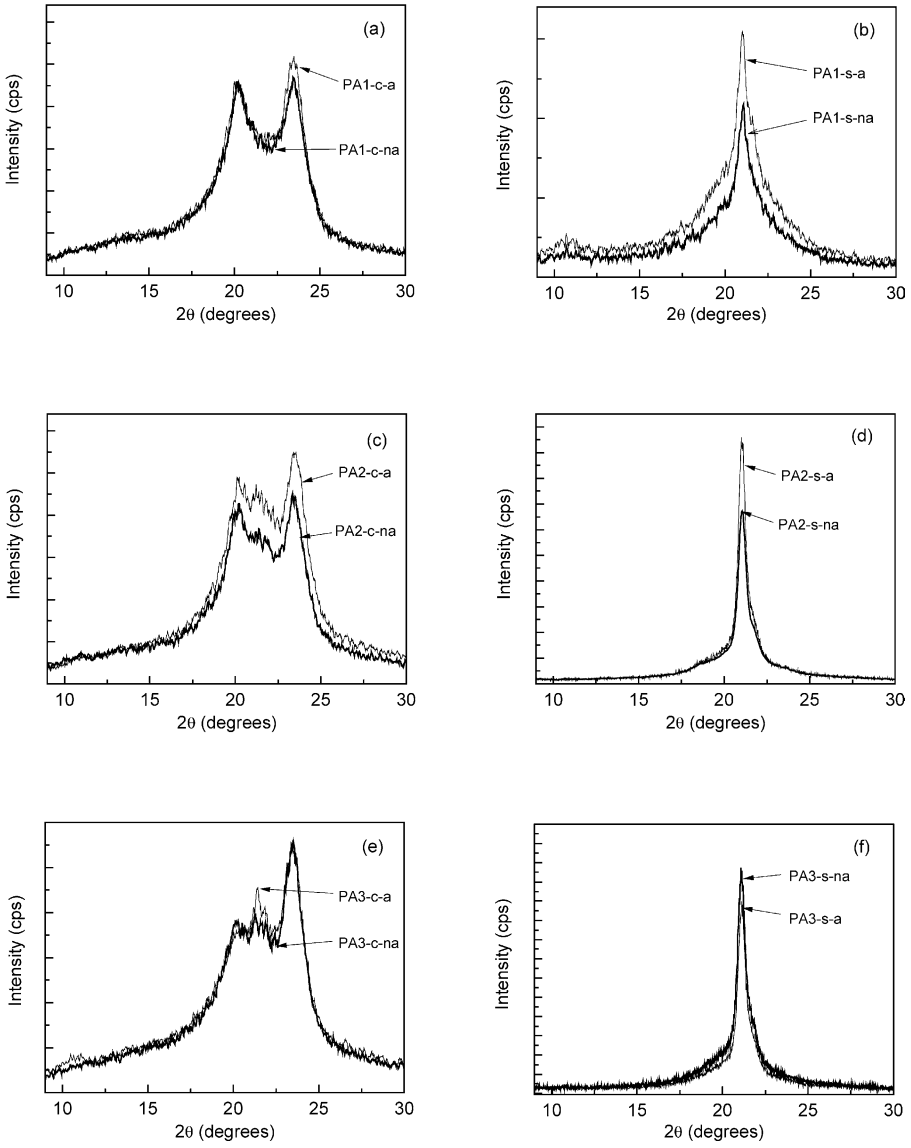

Fig. 7. WAXD patterns obtained from (a, c, e) core and (b, d, f) skin regions of injection-molded bars made from PA1, PA2 and PA3.

respectively:

$$X_{\text{C–WAXD}}(\%) = \frac{\sum(A_{\alpha\text{–form}} + A_{\gamma\text{–form}})}{\sum(A_{\alpha\text{–form}} + A_{\gamma\text{–form}}) + A_{\text{amorph}}} \times 100 \quad (3)$$

$$X_{\alpha\text{–WAXD}}(\%) = \frac{\sum A_{\alpha\text{–form}}}{\sum(A_{\alpha\text{–form}} + A_{\gamma\text{–form}}) + A_{\text{amorph}}} \times 100 \quad (4)$$

$$X_{\gamma\text{–WAXD}}(\%) = \frac{\sum A_{\gamma\text{–form}}}{\sum(A_{\alpha\text{–form}} + A_{\gamma\text{–form}}) + A_{\text{amorph}}} \times 100 \quad (5)$$

where, $A_{\alpha\text{-form}}$ and $A_{\gamma\text{-form}}$ are the areas below the α-form

Table 3
Crystallinity data calculated from WAXD spectra of injection-molded N6 samples

Sample	$X_{\alpha\text{-WAXD}}$ (%)	$X_{\gamma\text{-WAXD}}$ (%)	$X_{\text{C-WAXD}}$ (%)	$\gamma/(\alpha+\gamma)$ (%)
PA1-s-na	0	20.9	20.9	100
PA1-s-a	0	22.2	22.2	100
PA1-c-na	35.6	7.6	43.2	17.6
PA1-c-a	37.5	7.9	45.4	17.4
PA2-s-na	0	37.2	37.2	100
PA2-s-a	0	42.9	42.9	100
PA2-c-na	31.2	10.5	41.7	25.2
PA2-c-a	32.5	13.6	46.1	29.5
PA3-s-na	0	37.9	37.9	100
PA3-s-a	0	38.4	38.4	100
PA3-c-na	28.3	12.5	40.8	30.6
PA3-c-a	28.9	15.5	44.4	34.9

crystal peaks and the γ-form crystal peaks, respectively; A_{amorph} is the area of the amorphous part. The crystallinity data calculated from the above formulas and $\gamma/(\alpha+\gamma)$ ratio are shown in Table 3. In comparison with Table 2, it is observed that the $X_{C\text{-}WAXD}$ values are different from $X_{C\text{-}DSC}$. This probably reflects the arbitrary use of a single value of ΔH_m^0 for N6 without specific information on the types and amounts of each crystal phase present (especially to the core regions) and the inherent averaging of crystalline content during crystallization from melting associated with the DSC method.

From Fig. 7 and Table 3, we can observe the following interesting features for PA2 and PA3 nanocomposites in contrast to the case in PA1:

- Firstly, the amount of the γ-form crystal in NCNs (PA2 and PA3) is much larger than in PA1, especially in the skin regions. This indicates that the presence of clay indeed favors the formation of γ-form crystal, regardless of Na-MMT or OMMT. The large fraction of γ-form should be a consequence of interaction between MMT layers and N6 chains.
- Secondly, as seen from the WAXD patterns of skin regions, the $(020)_\gamma$ diffraction peak at $2\theta = 11.0°$ disappears in PA2 and PA3 (Fig. 7(d) and (f)). The $(020)_\gamma$ diffraction is assigned to be the amide hydrogen-bonded layer [9]. This may indicate that the MMT platelets restrict the formation of the hydrogen-bonded sheets of γ-form crystal of N6.
- Thirdly, as seen from the WAXD patterns of core regions, a discernible difference in the intensity of diffraction peaks between α1 peak ($2\theta \approx 20.2°$) and α2 peak ($2\theta \approx 23.4°$) can be observed. For PA1 (Fig. 7(a)), both the α1 and α2 peaks are well distinguishable. In the presence of Na-MMT, the intensity of α1 peak decreases in the core of PA2 (Fig. 7(c)). In the case of PA3 which contains OMMT instead of Na-MMT, the α1 peak is quite low in its core region (Fig. 7(e)). The α1 peak originates from the distance between hydrogen-bonded N6 chains, while the α2 peak comes from the separation distance between hydrogen-bonded sheets [4]. Therefore, the results may indicate that the MMT platelets also restrict the formation of the layered hydrogen-bonded sheets of α-form crystal of N6.

The increase of the total crystallinity of N6 after annealing can also be found in Table 3. In the skin regions there consisted of only γ-form crystals, the absolute content of γ-crystals increase after annealing with more increment for PA2, which is attributed to the perfection of crystals during annealing. After the annealing treatment, interestingly, the relative content of γ-form largely increases in the core regions of NCNs (PA2 and PA3), while the increment in pure N6 (PA1) can be hardly found. In the core of PA2, annealing leads to the increase of the fraction of α- and γ-form crystals simultaneously, with more increment of γ-form. However, it seems that annealing only increases the fraction of only one type of the crystals for the other samples: concretely, γ-form for PA3 and α-form for PA1.

4. Discussion

The double melting peaks are quite common in DSC measurements of N6 samples containing both α- and γ-form crystallines. In the absence of clay, the γ-form is reported to have a melting point about 8 °C below that of the α-form [3]. In the DSC heating curves of NCNs, some researchers [5,8] have suggested that the lower melting peak belongs to the γ-form and that the higher one belongs to the α-form. As well known and shown in this work, clay can indeed induce γ-form crystals in NCNs. Therefore, one would have no difficulty to understand that the low-temperature melting peak appears in the core region of PA2 or PA3, and that the enthalpy of the peak at 210 °C increases in the skin region of PA2 or PA3. But the question remains; i.e. the skin regions present only the γ-form. Although it is possible that the γ-form crystals can re-crystallize to the α-form during the DSC heating scans [31,32], it is not likely that so many γ-form crystals would re-crystallize to α-form at such fast heating rates (20 °C/min) [16]. The likely explanation is that the low-temperature endothermic peaks are only associated with smaller crystal structure and some imperfect crystal structure [15]. The presence of MMT platelets disrupts the crystal lamella organization and impedes large crystalline domains from forming due to steric hindrances, and leads to smaller, less ordered crystallites, and as a result, produces crystallites with a great distribution of size and shape. The larger shear stresses and higher cooling rates in the skin regions in comparison with the core regions lead to more imperfect crystallites.

The processing-induced mechanical stresses [25], or a γ/α transition in the absence of stress [31,32] can induce the sub-T_m transition in N6. In order to determine the origin of the recrystallization exotherm around 195 °C in this study, we investigated the melting behaviors of N6 samples with different processing history. The DSC heating scans are

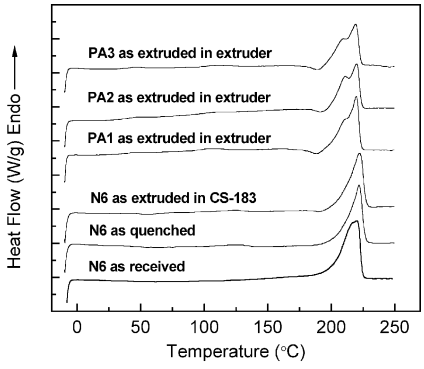

Fig. 8. DSC heating scans of N6 samples with different processing history. The curves are vertically offset for clarity.

shown in Fig. 8. The processing-induced memory effects in N6 can be obviously observed. Both of the as-received N6 and the quenched N6 did not present exothermic peaks, whereas a minor exothermic peak appeared in the extruded N6 in CS-183 once a small shear stress was imposed on the N6 melt. When larger shear stress was imposed on the extruded PA1 in twin-screw extruder, a melting shoulder peak at 211 °C and a deeper melting exothermic peak appeared. As indicated by Khanna et al. [25], the presence of the 195 °C exothermic transition is due to the release of the frozen-in strain energy absorbed during melt processing. It seems that our results support their interpretation. The frozen-in stresses might be located in the inter-lamellar regions through hydrogen bonding. These highly oriented polymer chains formed under the severe shear forces become mobile at the pre-melt temperatures. These chains reorganize and crystallize during DSC heating scans; as a result, some smaller and imperfect crystallites result partly in the low-temperature endothermic peak in the extruded PA1 in twin-screw extruder. As mentioned previously, it must be emphasized that the peak at approximately 210 °C is not necessary to be attributed to the γ-form crystalline. A recent study indicated that the mechanical shear of the pure N6 favors the formation of the α-form crystal under non-isothermal crystallization conditions [10]. In comparison with the extruded N6 in CS-183, the extruded N6 in twin-screw extruder could not present more γ-form crystals, because the thermal effects are similar in both cases and there is more significant shear effect in the latter case.

The effects of MMT on the melting behaviors of extruded PA2 and PA3 in twin-screw extruder were similar to the results of the skin regions of injection-molded NCNs (Fig. 5(b)). Interestingly, NCNs presented a little higher exothermic peak temperature than PA1 (Figs. 5(b) and 8) during DSC heating scans. We speculate that a portion of highly oriented polymer chains were trapped between the clay layers and impeded from crystallizing due to limited space. These polymer chains were kept in this metastable state up until higher sub-T_m than PA1 to crystallize. Previous studies have shown that a partially disordered structure of N6, intermediate metastable state, whose reversibility depends on a critical value of stress, also existed [33]. This metastable state was referred to the phase intermediate between α-form and γ-form. Regarding to this metastable state, it has to be realized that the frozen-in stresses could be located in the metastable state and the recrystallization exothermic transition is relevant to the presence of this metastable state. As a result, the double melting peaks are due to the existence of a series of crystal structures (including the metastable crystal structure and reorganization of crystals during DSC scanning), which vary continuously in size and perfection. The sub-T_m transition cannot be eliminated by annealing below such a temperature [25]. As can be observed from Figs. 5(d) and 9, this sub-T_m still existed in the N6 containing samples after annealing at 80 °C, but disappeared in the second DSC heating run after melting for 10 min at 280 °C.

Fig. 10 shows the DSC cooling scans of extruded N6 samples. Similar to the results of injection-molded N6 (Fig. 6), the introduction of MMT layers results in higher crystallization temperature, which is attributed to the heterogeneous nucleation of MMT. The presence of MMT can obviously facilitate nucleation of the N6 crystallites [12, 29], but the exothermic peak positions for PA2 and PA3 only show 1–3 °C higher than that of PA1. As reported by Fornes et al. [15], very small amounts (typical lower than 2 wt%) of clay increased the crystallization rate of N6, however, higher clay concentrations (~7 wt%) even reduced the crystallization rate due to hindered chain mobility by more clay particles. It is likely that the intermediate amounts (approximately 3 wt%) of MMT cannot greatly increase the crystallization temperature. The crystallization temperature of PA2 is slightly higher than that of PA3, which probably indicates that crystal growth in the exfoliated PA3 is more restricted than in the intercalated PA2.

It is well recognized that the presence of clay promotes the formation of γ-form of N6. Vaia et al. [9] indicated that the addition of clay layers forces the amide groups of N6 out of the plane formed by the molecular chains, which results in the conformational changes of the chains and restricts the formation of hydrogen-bonded sheets so that the γ-form is favored. In consideration of the intercalated/exfoliated nanostructure of NCNs (Fig. 3), the MMT layers hindered the polymer chains mobility leading to poor incorporation of the chains into the lamellar structure during crystallization, resulting in a limited formation of the hydrogen-bonded sheets of α- and γ-form. It seems that the exfoliation of MMT in N6 matrix accelerates this restrain, and promotes the formation of γ-form, which can also be seen after the annealing treatment. Some studies have found that the incorporation of MMT layers can weaken the hydrogen bonds in both the α- and γ-form crystalline of N6 [9,34]; however, it seems that no coincident conclusion has been drawn on the strength of hydrogen bonding [34–37]. Understanding the hydrogen bonding in our N6/Na-MMT and N6/OMMT requires further studies that are being carried out.

As mentioned above, annealing at 80 °C leads to an increase of the absolute content of γ-form in the skin regions and the relative content of γ-form in the core regions of PA2 and PA3. Considered that N6 has a glass transition temperature at around 50 °C [25], the mobility of the chain segments will be enhanced when annealed at 80 °C, leading to a reorganization of the chain segments in the amorphous regions around the γ-form crystallites. It should be noted that annealing did not enhance growth of α-form crystallites in the core of PA3 since the present α-form could also serve as growth templates. Mathias et al. [38,39] reported that while both crystal forms were present in NCNs, annealing at 200 °C under vacuum produced only

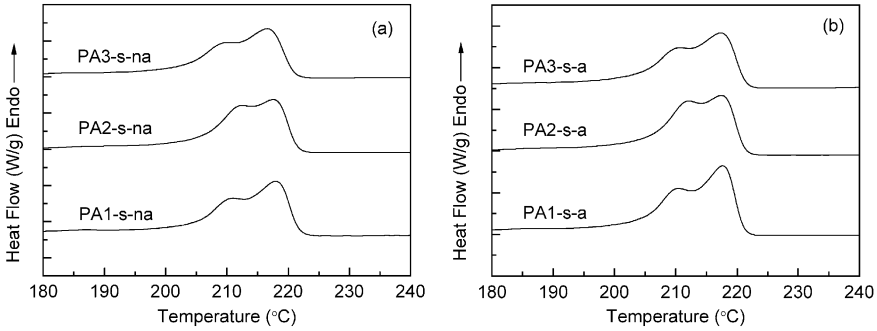

Fig. 9. Second heating DSC curves of samples taken from the skin regions of injection-molded PA1, PA2 and PA3 bars. The curves are vertically offset for clarity.

γ-form crystals. They considered that interfacial polymer/clay interactions induced the γ-form. The polymer chains did not array on the clay surface at an inter-chain distance that allowed formation of the layered hydrogen-bonded sheets of α-form, so the γ-form was generated. Though our annealing temperature is only 80 °C, the mechanism should be similar in the generation of γ-form during annealing. In the present work, we found that after the annealing treatment, (1) for the exfoliated PA3, only the fraction of γ-form increased; (2) for the intercalated PA2, the fraction of α- and γ-form crystals increased simultaneously, with more increment of γ-form; and (3) the fraction of α-form only increased for the neat PA1. We believe that this priority of crystallites growth to γ-form for PA3 during annealing at 80 °C could result from the confining crystallization environment, which limits the formation of hydrogen-bonded sheets of α-form, and that this confining effect is of kinetics origin [13,38]. That is, because the silicate platelet has a strong interaction with the polymer chains, N6 polymer chains mobility is greatly decreased. It was also reported that annealing at 190 °C produced more γ-form crystals in NCNs [40]. Obviously annealing at lower temperature (such as 80 °C in our work) can also favor the formation of γ-form crystallites in NCNs.

Annealing after injection molding can develop different crystallite morphologies for N6 and NCNs. With regard to the polymorphic structure of N6, the α-form crystalline is thermodynamically stable and the γ-form is metastable. Ito et al. [41] observed that the mechanical properties of the two crystalline phases, as well as the temperature dependence, were different. The α-form exhibits a higher modulus below T_g but a more rapid decrease above T_g than the γ-form. This implies that the γ-form has a higher heat distortion temperature (HDT). The increase in the degree of crystallinity (especially that of the γ-form) during annealing after injection molding will lead to different thermo-mechanical properties (especially to HDT [12,13]). These results will be reported in the forthcoming paper.

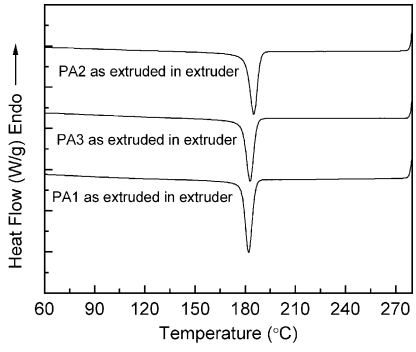

Fig. 10. DSC cooling scans of extruded N6 samples. The curves are vertically offset for clarity.

5. Conclusions

Intercalated N6/Na-MMT and exfoliated N6/OMMT nanocomposites were prepared by melt-compounding N6 with Na-MMT and organically modified MMT (OMMT), respectively. WAXD and DSC studies were carried out for the extruded and injection-molded pure N6 and nylon-6/clay nanocomposites (NCNs) specimens to understand the effects of processing history and annealing treatment on the thermal property and polymorphic structure of NCNs. The following conclusions were derived from the experimental results.

(1) Multiple melting behaviors were observed in the extruded and injection-molded pure N6 and NCNs specimens. Particularly a small exothermic peak around 195 °C just before the lower melting peak has been observed in the skin region. The influence of the processing history on the polymorphic structure of N6 can be manifested by itself in part. The experimental data clearly suggested that this sub-T_m transition should be attributed to the processing-induced shear stresses.
(2) Annealing at a temperature (80 °C) above the T_g of N6 after injection molding developed different crystallite morphologies for N6 and NCNs, as well as increasing the degree of crystallinity. In the skin regions there consisted of only γ-form crystals, the absolute content of γ-crystals increased after annealing. Meanwhile, the annealing treatment largely increased the relative content of γ-form in the core regions of NCNs. In

particular, annealing only increased the fraction of γ-form in the exfoliated N6/OMMT nanocomposites. It seems that this priority of crystallites growth to γ-form in the exfoliated NCNs during the annealing treatment resulted from the confining crystallization environment, which limited the formation of hydrogen-bonded sheets of α-form.

Acknowledgements

The authors are grateful to Major Basic Research Project of China for the financial support (Grant G2003CB615600).

References

[1] Ray SS, Okamoto M. Prog Polym Sci 2003;28:1539–641.
[2] Kawasumi M. J Polym Sci, Part A: Polym Chem 2004;42:819–24.
[3] Murthy NS, Aharoni SM, Szollosi AB. J Polym Sci Polym Phys Ed 1985;23:2549–65.
[4] Murthy NS, Curran SA, Aharoni SM, Minor H. Macromolecules 1991;24:3215–20.
[5] Wu TM, Liao CS. Macromol Chem Phys 2000;201:2820–5.
[6] Kojima Y, Usuki A, Kawasumi M, Okada A, Fukushima Y, Kurauchi T, et al. J Mater Res 1993;8:1185–9.
[7] Kojima Y, Usuki A, Kawasumi M, Okada A, Kurauchi T, Kamigaito O, et al. J Polym Sci, Part B: Polym Phys 1995;33: 1039–45.
[8] Liu L, Qi Z, Zhu X. J Appl Polym Sci 1999;71:1133–8.
[9] Lincoln DM, Vaia RA, Wang ZG, Hsiao BS. Polymer 2001;42: 1621–31.
[10] Medellin-Rodriguez FJ, Burger C, Hsiao BS, Chu B, Vaia RA, Phillips S. Polymer 2001;42:9015–23.
[11] VanderHart DL, Asano A, Gilman JW. Chem Mater 2001;13: 3781–95.
[12] Maiti P, Okamoto M. Macromol Mater Eng 2003;288:440–5.
[13] Lincoln DM, Vaia RA, Wang ZG, Hsiao BS, Krishnamoorti R. Polymer 2001;42:9975–85.
[14] VanderHart DL, Asano A, Gilman JW. Chem Mater 2001;13: 3796–809.
[15] Fornes TD, Paul DR. Polymer 2003;44:3945–61.
[16] Yalcin B, Cakmak M. Polymer 2004;45:2691–710.
[17] Masenelli-Varlot K, Reynaud E, Vigier G, Varlet J. J Polym Sci, Part B: Polym Phys 2002;40:272–83.
[18] Uribe-Arocha P, Mehler C, Puskas JE, Altstädt V. Polymer 2003;44: 2441–6.
[19] Cho JW, Paul DR. Polymer 2001;42:1083–94.
[20] Fornes TD, Yoon PJ, Keskkula H, Paul DR. Polymer 2001;42: 9929–40.
[21] Kojima Y, Usuki A, Kawasumi M, Okada A, Kurauchi T, Kamigaito O, et al. J Polym Sci, Part B: Polym Phys 1994;32:625–30.
[22] Yu ZZ, Yang M, Zhang Q, Zhao C, Mai YW. J Polym Sci, Part B: Polym Phys 2003;41:1234–43.
[23] Yalcin B, Valladares D, Cakmak M. Polymer 2003;44:6913–25.
[24] Morgan AB, Gilman JW. J Appl Polym Sci 2003;87:1329–38.
[25] Khanna YP. Macromolecules 1992;25:3298–300.
[26] Khanna YP, Kuhn WP. J Polym Sci, Part B: Polym Phys 1997;35: 2219–31.
[27] Wu Q, Liu X, Berglund LA. Macromol Rapid Commun 2001;22: 1438–40.
[28] Campoy I, Gómez MA, Marco C. Polymer 1998;39:6279–88.
[29] Lincoln DM, Vaia RA, Krishnamoorti R. Macromolecules 2004;37: 4554–61.
[30] Gurato G, Fichera A, Grandi FZ, Zanetti R, Canal P. Makromol Chem 1974;175:953–75.
[31] Penel-Pierron L, Depecker C, Séguéla R, Lefebvre JM. J Polym Sci, Part B: Polym Phys 2001;39:484–95.
[32] Medellín-Rodríguez FJ, Larios-López L, Zapata-Espinoza A, Dávalos-Montoya O, Phillips PJ, Lin JS. Macromolecules 2004; 37:1799–809.
[33] Murthy NS. Polym Commun 1991;32:301–5.
[34] Wu Q, Liu X, Berglund LA. Polymer 2002;43:2445–9.
[35] Lu Y, Zhang G, Feng M, Zhang Y, Yang M, Shen D. J Polym Sci, Part B: Polym Phys 2003;41:2313–21.
[36] Zhang G, Li Y, Yan D. J Polym Sci, Part B: Polym Phys 2004;42: 253–9.
[37] Chen G, Shen D, Feng M, Yang M. Macromol Rapid Commun 2004; 25:1121–4.
[38] Mathias LJ, Davis RD, Jarrett WL. Macromolecules 1999;32: 7958–60.
[39] Davis RD, Jarrett WL, Mathias LJ. In: Krishnamoorthy R, Vaia RA, editors. Polymer nanocomposites: synthesis, characterization, and molding. Washington, DC: American Chemical Society; 2001. p. 117–26.
[40] Hu X, Zhao X. Polymer 2004;45:3819–25.
[41] Ito M, Mizuochi K, Kanamoto T. Polymer 1998;39:4593–8.